Applied Catalysis B: Environmental 125 (2012) 465–472

Contents lists available at SciVerse ScienceDirect

Applied Catalysis B: Environmental

journal homepage: www.elsevier.com/locate/apcatb

# Photoelectrochemical degradation of azo dye over pulsed laser deposited nitrogen-doped $TiO_2$ thin film

Yen-Ping Peng[b], Emre Yassitepe[c], Yun-Ta Yeh[a], Inci Ruzybayev[d], S. Ismat Shah[c,d], C.P. Huang[a,*]

[a] Department of Civil and Environmental Engineering, University of Delaware, Newark, DE 19716, USA
[b] College of Environmental Science and Engineering, South China University, 510006 PR China
[c] Department of Material Science Engineering, University of Delaware, Newark, DE 19716, USA
[d] Department of Physics and Astronomy, University of Delaware, Newark, DE 19716, USA

ARTICLE INFO

*Article history:*
Received 23 January 2012
Received in revised form 5 June 2012
Accepted 12 June 2012
Available online 20 June 2012

*Keywords:*
Photoelectrochemical
Pulsed laser deposition
N-doped $TiO_2$
Thin film
Synergetic effect

ABSTRACT

We investigated the synergetic effect of electrochemical and photocatalytic oxidation in photoelectrochemical (PEC) process for the degradation of hazardous organic compounds exemplified by methyl orange, an azo dye. Nitrogen doped $TiO_2$ thin film (NTTF) synthesized by the pulsed laser deposition (PLD) method, was used as the working anode. The crystalline, optical properties, surface morphology, and structure of the NTTF were characterized by XRD, UV–vis absorbance edges, SEM, and XPS. Results showed that the NTTF was dominated by anatase phase after sintered at 600 °C with significant visible light response at 595 nm. XPS analyses indicated nitrogen doping was mainly responsible for reducing the band gap as evidence of 3% N doping into the structure via the linkage of Ti—O—N and N—Ti—O bond. SEM images illustrated the nitrogen-doped $TiO_2$ nanoparticles being attached firmly and spread evenly over the ITO glass surface, which is beneficial for PEC applications. The degradation efficiency of MO by photoelectrochemical, photocatalytic, electrochemical and photolysis methods were compared in terms of pseudo-first-order reaction rate. PEC was the most efficient in degrading MO at a bias potential of 2.0 V (vs. SCE) under light at a wavelength of 325 nm, which was consistent with results of IPCE (%) measurements. The synergetic effect was quantified at current/bias potential of 0.07 mA/0.3 V and 0.6 mA/2.0 V, respectively. Results demonstrated that the bias potential could separate photogenerated holes and electrons effectively and enhance the electrochemical-oxidation of MO. The mechanistic aspects of MO degradation by the PEC process were discussed.



## 1. Introduction

Semiconductors have been intensively investigated for applications in water splitting, solar cell, and pollutant degradation [1–3]. Among the various semiconductors, titanium dioxide ($TiO_2$) has received the most attention due to its attractive photocatalytic activity, chemical stability, nontoxicity, and low cost [2,3]. However, $TiO_2$ has a relatively large band gap, between 3.2 and 3.4 eV, which impedes its applications. In other word, $TiO_2$ is excitable only by UV light, which occupies less than 5% of the solar spectrum. Furthermore, in the absence of electron and hole scavengers, after photoexcitation the stored energy is dissipated due to rapid electron–hole recombination, within a few nanoseconds, to yield a neutral state through emission of photons in a volumetric or surface level [2,4]. This electron–hole recombination process not only suppresses the quantum efficiency but also decreases the oxidation capability of semiconductors.

A great deal of efforts have been made to modify the band gap of $TiO_2$ by size control [5–7], manipulating the oxygen vacancy [8,9], and doping impurities [10]. Asahi et al. [11] were among the first investigators to demonstrate that, among nonmetal dopants such as C, N, F, P and S, the substitution doping of N was the most effective because its p states contribute to the band gap narrowing by mixing with the O 2p state. Results showed that films and powders of $TiO_{2-x}N_x$ have improved the optical absorption over that of titanium dioxide under visible light (wavelength < 500 nm). Therefore, considerable efforts have been made to dope $TiO_2$ powders, nanotubes, and thin films with N [12–20]. Among these various types of N-doped $TiO_2$ materials, thin film shows superior utility and feasibility due to its convenience for reuse and recycling. Several $TiO_2$ thin film deposition techniques including sol–gel [21], electrophoretic deposition [22], metalorganic chemical vapor deposition (MOCVD) [23], and pulsed laser deposition (PLD) [12,16–20,24,25] have been conducted. PLD is a high-energy process which provides a well adherent thin film with good

* Corresponding author. Tel.: +1 302 831 8428; fax: +1 302 831 3640.
*E-mail address:* huang@udel.edu (C.P. Huang).

0926-3373/$ – see front matter © 2012 Published by Elsevier B.V.
http://dx.doi.org/10.1016/j.apcatb.2012.06.004

mechanical rigidity [26] and high specific surface area. Moreover, PLD provides advantages such as transferring material from target to substrate stoichiometrically [26], operating in wide range of pressure and temperature, and versatility in the selection of substrate materials. Many studies has successfully synthesized N-doped $TiO_2$ thin film by PLD method [12,16–20], however, most of these studies had focus on the material fabrications and characterization. In the present study concentration was on the potential environmental applications of NTTF.

To minimize the hole–electron recombination, the PEC method, a combined electrochemical and photocatalytic oxidation, was applied to separate the electrons and the holes by applying a bias potential across the anode and the cathode. Presently, PEC systems have been widely studied in many areas including solar cell [27,28], hydrogen generation [29–32], $CO_2$ reduction [33–36] and water remediation [37–44]. Generally, the PEC process, with an externally applied bias potential, enables electrochemical oxidation of chemical pollutants and promotes photocatalysis as well by removing the electrons from and providing oxygen to the anodic region. The synergetic effect of electrochemical and photocatalytic oxidation in PEC system has been investigated by various research groups with good qualitative understanding of how reactions occur [44–46]. However, more quantitative information on factors contributing to the synergetic effect in the PEC system is needed.

This present study was to synthesize nitrogen doped $TiO_2$ thin film using PLD method and to apply the NTTF photocatalyst in a PEC system for the treatment of organic compounds exemplified by methyl orange (MO), an azo dye. The NTTF was characterized with scanning electron microscopy (SEM), X-ray diffraction patterns (XRD), X-ray photoelectron spectroscopy (XPS), and UV–vis diffuse reflectance spectroscopy (DRS). The synergetic effect and mechanism for the degradation of MO using the PEC system were discussed.

## 2. Experimental

### 2.1. N-doped $TiO_2$ thin film preparation

Pure $TiO_2$ target was prepared from P25 Degussa particles (Sigma–Aldrich, USA). The target was ablated under partial Nitrogen and Oxygen atmosphere on an ITO coated glass (SPI supplies Inc., PA, USA) by PLD technique. The description about the apparatus setup was given by Lin et al. [25] in details. Briefly, a KrF excimer laser (Lambda physic LPX 305, $\lambda = 248$ nm) was applied. Base pressure in the system was kept below 0.01 Pa with a turbo molecular pump and a mechanical pump. A mixture of $N_2$ and $O_2$ (4:1) was purged to the system, while the chamber pressure was maintained at 13.3 Pa. Two 500-W halogen lamps were used as irradiative heating source to control the substrate temperature up to 600 °C. Eventually, the target was ablated for 20 min.

### 2.2. Characterization

The microstructure and morphology of the synthesized materials were observed with a scanning electron microscopy (SEM, JSM 7400F). The crystal structures of $TiO_2$ thin film (TTF) and NTTF were characterized by X-ray diffraction (Rigaku D-Max B) with Cu Kα radiation ($\lambda = 1.54$ Å) operating at a voltage of 30 kV and a current of 30 mA. Samples were analyzed by Brag Brentano geometry and are scanned with 0.02-step size between 20° and 80°. The crystal structures were solved by maud software using rietveld method. UV–visible spectroscopy, collecting transmission and reflectance data by Perkin Elmer instruments (Lambda 750), was applied to investigate the absorbance spectra of NTTF over a range of 300–800 nm. X-ray photoelectron spectra were collected with Omicron surface science instruments. High resolution XPS spectra of N 1s, Ti 2p and C 1s regions were collected with a step size of 0.02 and 0.2 s of dwell time. The resulting spectra were fitted by XPSPEAK with Shirley background. Furthermore, high resolution XPS analysis of Ti, O, and N were conducted with spectra signal collected and convoluted. The nitrogen atomic content was obtained based on the relative ratio of the peak area and atomic sensitivity factors of all elements. The whole nitrogen spectrum was summed and the percent N doped estimated.

### 2.3. PEC and electrochemical measurements

All PEC experiments were carried out in a three-electrode system. A saturated calomel electrode (SCE) was selected as the reference electrode. The NTTF was used as the working electrode (6.25 $cm^2$) and a copper wire (Fisher Scientific, 155451A-16AWG-B16, od: 1 mm, length: 163 cm, total surface area: 51.2 $cm^2$), pretreated by switched potential of 10 V in 0.1 M $H_2SO_4$ (Fisher Scientific, USA), was used as the counter electrode. The electrolytes were 0.1 M NaCl (ACROS, USA) and 0.1 M $KHCO_3$ (Fisher Scientific, USA) in anodic and cathodic chambers, respectively. A self-designed H-type reactor was made to separate the anode and cathode for better evaluation for the MO degradation. These two chambers were connected with a cation-exchanged membrane to keep the ion balance in the system. A quartz window (7 $cm^2$), on the side of the anode chamber, was used to provide good optical quality. The potential for both current–potential measurements and PEC degradation experiments was controlled by a potentiostat (Model AFRDE 4, Pine Instrument Inc., USA). Monochromatic excitation source (Model RF-5301, Shimadzu, Japan) was applied as the light source for photo-activities tests of NTTF. For PEC degradation experiments, the light source was 100-W Xe lamp with the average intensity of incident light of 3.12 mW $cm^{-2}$, measured by a high sensitivity thermal sensor (Model 3A-P-SH-V1, OPHIR, USA).

## 3. Results and discussion

### 3.1. Characterization of N-doped $TiO_2$ thin film

Fig. 1 shows results of the XRD characterization of the N-doped $TiO_2$ thin film and pure $TiO_2$ thin film. After sintered at 600 °C, both NTTF and TTF structures showed peaks at 25°, 38°,

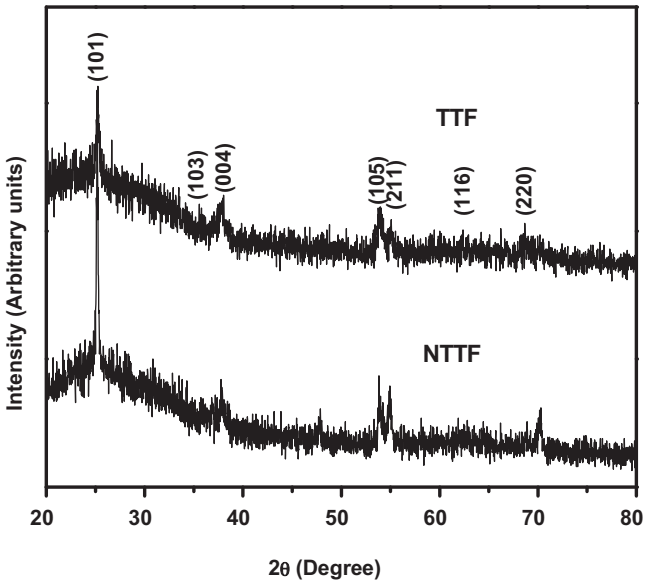


**Fig. 1.** XRD patterns of TTF and NTTF.

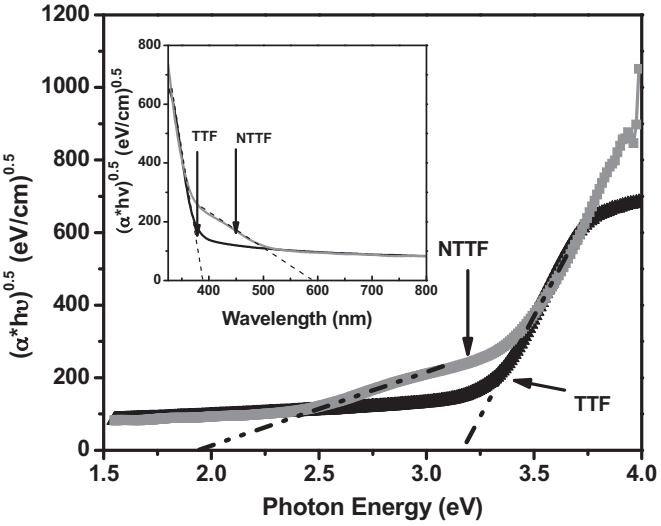


**Fig. 2.** Characterization of band gap for TTF and NTTF. Inset plot shows the UV–vis absorbance of TTF and NTTF.

54° and 63° corresponding to anatase phase. This crystal structure matched with JCPDS-784486. No rutile peak appeared in either of the two samples based on XRD results due to insufficient sintered temperature. Generally, rutile is more densely packed and thermodynamically stable than anatase [47], whereas the latter is considered the more photoactive form of $TiO_2$. The lattice constants were $a = 3.7993 \pm 0.0009$ and $c = 9.4983 \pm 0.004$ for NTTF and $a = 3.7806 \pm 0.002$ and $c = 9.4893 \pm 0.009$ for TTF; the above values matched closely with those structures identified.

The absorption coefficient of the thin films was calculated with the following formula [48];

$$\alpha(h\nu) = -\frac{1}{d}\ln\left(\frac{T}{(1-R)^2}\right) \quad (1)$$

where $\alpha$ is the absorption coefficient, $d$ is the thickness of the film, $T$ is transmission at a particular wavelength, and $R$ is the reflectance characteristics of the film, i.e.,

$$\alpha(h\nu) \propto \frac{(h\nu - E_g)^n}{h\nu} \quad (2)$$

The optical band gap was calculated by plotting $(\alpha h\nu)^n$ vs. $h\nu$, where $n$ is 0.5 for indirect and 1 for direct band gap materials. The doping effect can be seen from the results of band gap characterization. From Fig. 2, both TTF and NTTF showed the characteristic band gap of 3.2 eV, which corresponds to anatase phase in titanium dioxide nanomaterial. Furthermore, NTTF showed a secondary slope at 2.0 eV, which was attributed to the additional states due to nitrogen doping [15,49–51]. As demonstrated in the inset plot in Fig. 2, the absorbance shoulders for NTTF exhibited high absorbance in longer wavelength at 595 nm, which indicated that NTTF could be excited in visible light region. The significant absorbance for visible light can be attributed to the O—Ti—N linkage, leading to the narrowing of energy band gap [11,51]. This phenomenon illustrated the formation of an intra-band gap located above the valence band, due to the interstitial introduction of nitride into the oxide lattice and/or to substitution of oxide centers by nitride centers [52].

Fig. 3 shows the SEM images collected for surface and cross section of the TTF and NTTF. Results showed continuous and uniform area with columnar grains with an average thickness of 545 and 640 nm for NTTF and TTF, respectively. This illustrated the firm attachment and even spreading of nitrogen-doped $TiO_2$ nanoparticles on the ITO glass, which is beneficial to wide industrial applications. The surface images revealed that TTF (100 nm) had a larger grain size and rougher surface than NTTF (60 nm). The differences resulted could be attributed to the different gases employed in the synthesis procedure. Only oxygen gas was employed in the TTF synthesized process, however a blend gas of nitrogen and oxygen with a mixed ratio of 4:1 was purged into the system for NTTF synthesis. The non-uniformity could arise from the bond breaking of the molecular gaseous precursors. Similar results were observed for carbon-doped titanium dioxide thin film as reported in our previous study [29].

In order to analyze the states of the chemical bonding (and surface concentration of Nitrogen) near the film surface, two XPS high resolution-scan spectra, Ti 2p (Fig. 4a), and N 1s (Fig. 4b), were investigated. Fig. 4a shows results of high resolution XPS spectra for Ti 2p. It could be seen that Ti 2p spectra of NTTF consists of two peaks at around 459.5 eV (Ti $2p_{3/2}$) and 465.3 eV (Ti $2p_{1/2}$). Ti 2p region showed that Ti was in +4 state, which was confirmed by the oxidation of Ti to $TiO_2$. A Ti +3 state was also observed due to the vacancies created by the PLD procedure and nitrogen doping. In contrast to chemical-based synthesis (i.e., sol–gel and MOCVD), multi-valance Ti species are usually created during the PLD deposition process [25]. The N 1s spectra show a clear peak at 400 eV which represents the Ti—O—N bond and a vague peak at 396.5 eV which may refer to the N—Ti—O bond. The doping linkage may be different dependent on the synthesis methods and nitrogen sources. Ou et al. [51] used microwave assisted hydrothermal method to synthesize the N-doped $TiO_2$ by annealing the titanate nanotubes in a gaseous mixture ($Ar/NH_3$ for 80/20 vol%) at 500–700 °C. Results of XPS analysis showed clear N—Ti—O bond at 396.3 eV for $TNTiO_2$-70 W and $TNTiO_2$-700 W when the annealing temperature was above 600 °C. However, the Ti—O—N linkage merely appeared weakly when annealing temperature was above 700 °C.

Accordingly, the appearance of N 1s spectra in NTTF provides evidence that nitrogen was successfully doped into TiO2 structure by PLD method. In addition, the nitrogen concentration was 3% in the NTTF based on XPS analysis. From results of XPS and UV–vis analyses, we can see the band gap reduction created by the additional states from Nitrogen doping.

Notably, the color of samples sintered at 600 °C was yellow, which was indicative of the successful doping of N into $TiO_2$ lattice and good absorbance of visible light [15,51,53]. The above observation was consistent with results of XPS and UV–vis analyses.

### 3.2. Photoelectrochemical activities of NTTF

The photoelectrochemical efficiency of NTTF was measured in terms of incident photon conversion efficiency IPCE (λ). The IPCE (λ) is defined as the number of electrons transferred per incident photon (Eq. (3)),

$$\mathrm{IPCE}\,(\%) = \frac{J_{sc}(\lambda)}{eI_{inc}(\lambda)} = \left[1240\frac{J_{sc}\ (\mathrm{A\ cm^{-2}})}{e\lambda\,(\mathrm{nm})I_{inc}\,(\mathrm{W\ cm^{-2}})}\right] \times 100 \quad (3)$$

where the $J_{sc}(\lambda)$ is short-circuit photocurrent density under monochromatic light ($A\,cm^{-2}$), e is the electron charge (C), and $I_{inc}(\lambda)$ is the incident photon flux ($W\,cm^{-2}$). This method provides more information on the photocatalytic properties than optical absorption, due to the exclusion of surface morphology and mass transfer limitation effect in the latter method. The IPCE (λ) is a function of incident wavelength and is a measurement of quantum efficiency for a particular semiconductor photoelectrode. When applying a certain photon energy/wavelength, the obtained quantum efficiency represents the energy differences between the local electronic states and the conduction band minimum. Therefore, if there is no significant change in energy position of the conduction band minimum, the edge of the IPCE (λ) spectrum is

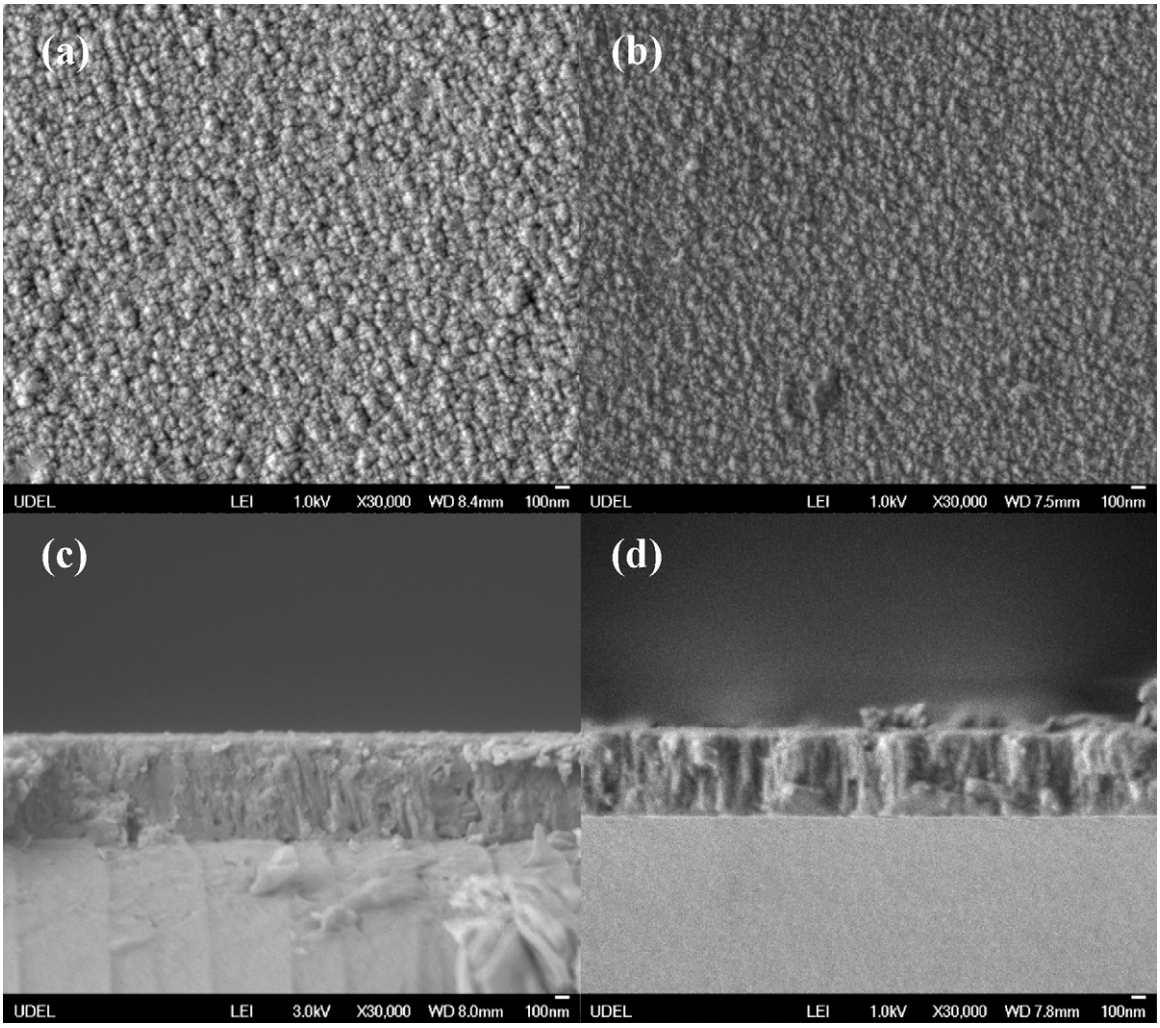


**Fig. 3.** SEM images of the surface of (a) TTF, (b) NTTF; cross-section images for (c) TTF and (d) NTTF.

qualitatively proportional to the density of states for the valance band maximum. In other words, the onset of the IPCE (λ) spectrum is similar to the wavelength of threshold bandgap ($\lambda_{bg}$) of a particular semiconductor.

The IPCE (λ) of NTTF were investigated at 0.3, 0.5, 0.7, 1.0, 1.5 and 2.0 V, and under irradiation wavelength from 300 to 425 nm with every 25 nm interval. As shown in Fig. 5, the IPCE (λ) value of NTTF increased with the increase in external potential applied. The highest photo-response was obtained at 325 nm, i.e., the maximum IPCE (λ) value of 26.77% was observed at the irradiation of 325 nm and a bias potential of 2.0 V (Table 1). Although the UV–vis results provide evidence that NTTF can be excited in visible light region, the IPCE results showed a better photo-electro response of NTTF at shorter irradiation wavelength. This might be that irradiation in shorter wavelength always has higher photo-energy. Higher photo-energy accompanies greater photon kinetic energy, which facilitates movement of photons. The IPCE for pure $TiO_2$ film was also calculated under the same conditions of irradiation and bias potential of 0.75 V as reported in our previous study [23]. It is noted that even though the band gap was expanded from 325 to 595 nm upon N doping, wavelength at 325 nm still yields the maximum photocatalytic degradation due to higher energy available for electron excitation. Generally, higher light energy accompanies more absorbed photons which can excite the photocatalyst to separate the electrons and holes, resulting in higher photoactivity. In contrast, NTTF expressed a photocurrent of 1.142 mA at 425 nm, whereas, the pure $TiO_2$ thin film photocurrent almost disappeared at 400 nm [29]. This illustrated that NTTF has better visible light response than pure $TiO_2$ thin film. Notably, the IPCE (λ) spectrum exhibited trends similar to UV–vis diffuse reflectance absorption; both showed two adsorption edges as evidence of that the IPCE (λ) function considers the effect of surface morphology and mass transfer limitation on the determination of band gap.

**Table 1**
IPCE(%) and photocurrent at various bias potential.

| $V_{bias}$ (vs. SCE, V) | 0.3 | 0.5 | 0.7 | 1.0 | 1.5 | 2.0 |
|---|---|---|---|---|---|---|
| Dark current (mA) | 0.023 | 0.160 | 0.292 | 0.413 | 0.517 | 0.607 |
| Photocurrent (mA) | 0.072 | 0.198 | 0.223 | 0.337 | 0.582 | 0.595 |
| Total current (mA) | 0.095 | 0.358 | 0.515 | 0.75 | 1.099 | 1.202 |
| Light intensity ($mW\,cm^{-2}$) | 7.6 | 7.6 | 7.6 | 7.6 | 7.6 | 7.6 |
| IPCE (%) | 2.93 | 8.06 | 9.08 | 13.72 | 23.70 | 26.77 |

### 3.3. Degradation of MO over N-doped $TiO_2$ thin film

Four MO removal processes, namely, PEC, photocatalytic (PC), electrochemical [6] and direct photolysis (P) processes were conducted to evaluate the degradation efficiency. The PEC, PC and photolysis experiments were examined at the illumination using 100-W Xe lamp at 3.12 $mW\,cm^{-2}$. The applied voltage in PEC and EC process was 2.0 V (vs. SCE), at which, both CV [54] and IPCE results yielded the best response with respect to

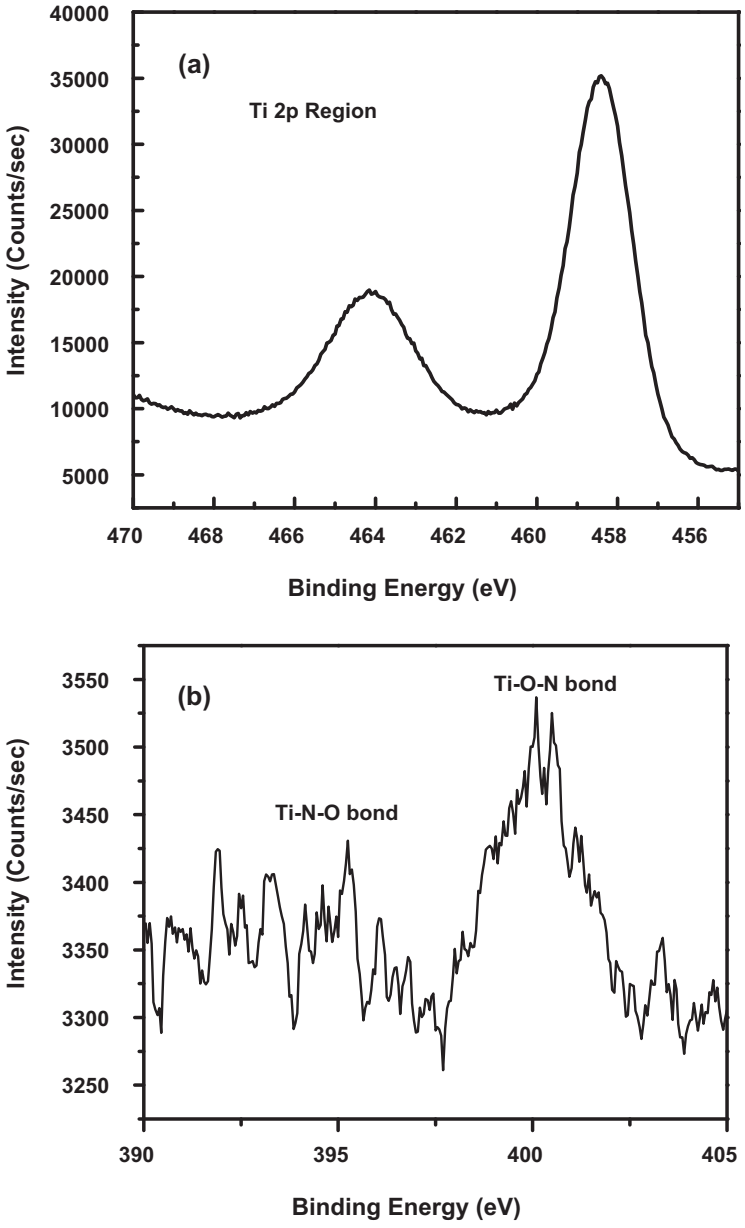


**Fig. 4.** High resolution XPS spectra for (a) Ti 2p, and (b) N1 s region of NTTF.

photocurrent-bias potential. In the range of bias potential studied, i.e., 0.3–2 V, the maximum photocurrent occurred at 2.0 V which appeared to agree with the results of cyclic voltammetric scans. As shown in Fig. 6, PEC process was the most efficient way to degrade MO among four methods studied. The complete removal of 1 mg/L of MO was observed after 40 min, whereas only 14.9, 36.3 and 5.1% of the MO removal was achieved by the PC, EC and P process within the same irradiation time, respectively. It was comprehensible that PEC method provided the most powerful way to degrade MO due to the combination of electrochemical oxidation and photocatalysis. Zhao et al. [44] successfully demonstrated the synergetic effect of combining electrochemical-oxidation and photolysis by using porous $ZnWO_4$ photoanode to oxidize dye, Rh-B. The results showed that when the bias potential was greater than 1.3 V, indirect electrochemical-oxidation of Rh-B occurred with the largest synergetic effect. Similar results were also shown in this study. As the bias potential was applied, the photocatalytic degradation of MO was enhanced by promoting the separation and isolation of photogenerated electrons and holes. Hole–electron separation enhanced not only the electrochemical oxidation but also the photocatalytic oxidation. For purpose of comparison, the MO degradation was 19.5 and 47.0% and the rate constant was $6.83 \times 10^{-5}$ and $1.52 \times 10^{-4}\,s^{-1}$ for PC and EC, respectively. The applied voltage in EC method is a key factor regarding the degradation efficiency. For example, Zhao et al. [46] applied $\gamma$-$Bi_2MoO_6$ film electrode to examine the oxidation efficiency of Azo dye via photocatalysis degradation (irradiated by 150-W Xe lamp) and electrochemical-oxidation (under bias potential of 3.0 V vs. SCE). Results showed that EC had better efficiency than PC. Hou et al. [55] studied the oxidation of Acid Orange Π using nano-$TiO_2$ particles coated onto activated carbon fibers ($TiO_2$/ACF) and compared the results of photoelectrochemical (PEC) and photocatalytic (PC) treatments. Results showed that PC (irradiated by 15-W $UV_{254}$ lamp) and PEC (under bias potential of 0.5 V vs. SCE) removed 77.8 and 90.0% AOΠ in 180 min, respectively. Above results illustrated that, as the applied bias potential was below the redox potential of the target compound, increase in bias potential could increase the photocatalytic ability by promoting the separation and

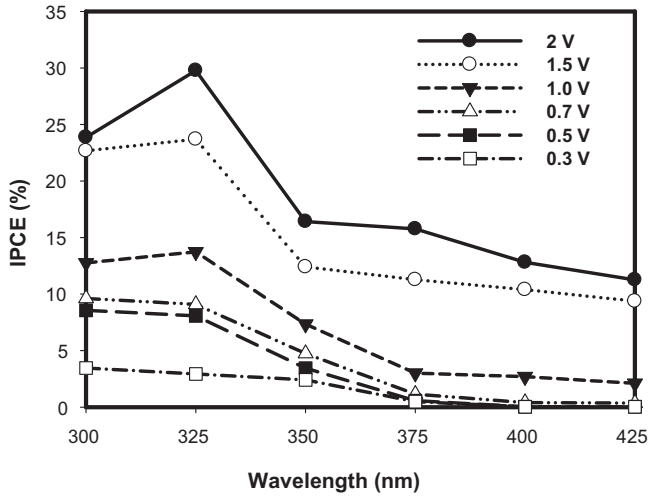


**Fig. 5.** IPCE (%) versus wavelength (300–425 nm) as a function of bias potential in 0.1 M NaCl electrolyte. Experimental conditions: working electrode = NTTF; reference electrode = SCE; counter electrode = Cu; electrolyte = 0.1 M NaCl (anode); electrolyte = 0.1 $MKHCO_3$ (cathode); pH 7.0 (anode); pH 8.3 (cathode); temperature = 298 K; light source = monochromatic excitation source (Model RF-5301, Shimadzu, Japan; 7.6 mW $cm^{-2}$).

transfer of photogenerated holes and electrons. On contrast, when the applied bias potential was greater than the redox potential of target compound, not only could it separate the holes and electrons but also could directly electrolyze the target compound [44]. The CV profile of the NTTF in 1 mg/L of MO and 0.1 M of NaCl electrolyte under irradiation (100 W Xe lamp) was reported previously [54]. When the bias potential exceeded 1.6 V, the current increased greatly, this may be brought by the electrochemical oxidation of MO and oxygen evolution reaction. Moreover, the photocurrent was potential dependent. It increased as the applied potential was scanned toward positive region (anodic), especially at potentials greater than 1.6 V, and gradually reached the maximum photocurrent (at 2.0 V). This implied that the photocurrent generated from the NTTF photoanode could be effectively driven to the counter electrode by this positive potential, which would favor charge separation. In two-chamber PEC system, applying potentials greater than the NTTF flat band potential under illumination condition

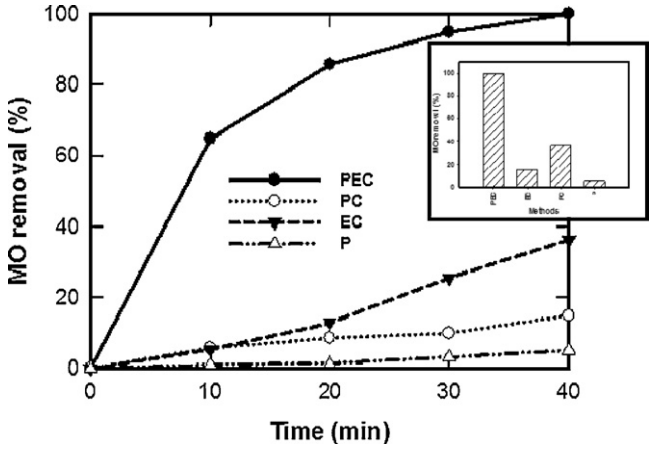


**Fig. 6.** Removal of MO by various oxidation processes including photoelectrochemical (PEC), photocatalytic (PC), electrochemical (EC), and photolytic (P) methods. Inset plot shows percent removal at 40 min. Experimental conditions: initial concentration of MO was 1 ppm; light source = 3.12 mW $cm^{-2}$ (100 W Xe lamp); working electrode = NTTF; reference electrode = SCE; counter electrode = Cu; bias potential = 2 V (vs. SCE); pH 6.0 (anode); pH 6.8 (cathode); electrolyte = 1 ppm MO in 0.1 M NaCl (anode); electrolyte = 0.1 M $KHCO_3$ (cathode); temperature = 298 K.

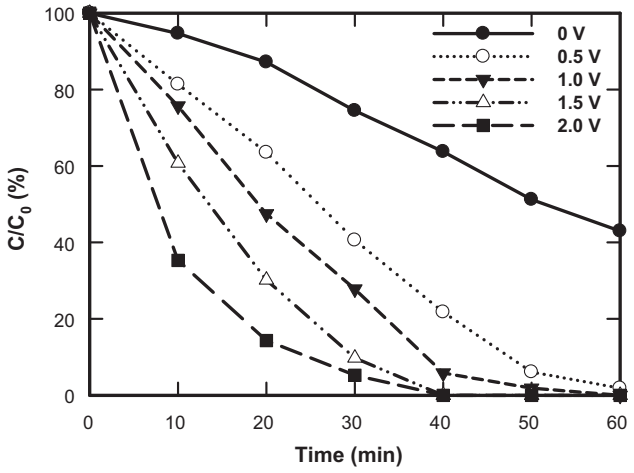


**Fig. 7.** Effect of bias potential on PEC degradation of MO. Experimental conditions: initial concentration of MO was 1 ppm; working electrode = NTTF; reference electrode = SCE; counter electrode = Cu; light source = 3.12 mW $cm^{-2}$ (100 W Xe lamp); pH 6.0 (anode); pH 6.8 (cathode); electrolyte = 0.1 M NaCl (anode); electrolyte = 0.1 M $KHCO_3$ (cathode); temperature = 298 K.

could transfer the photogenerated current via an external circuit to the cathode. This may increase the activity of photogenerated active species, e.g., holes, on the surface of photoanode by impeding the recombination between photogenerated holes and electrons. Moreover, no vibrational concentration was observed under darkness which implied that the adsorption effect could be ignored in the process.

### 3.4. Effect of bias potential for PEC

External potentials were applied at various vales (e.g., 0, 0.5, 1.0, 1.5 and 2.0 V) as to evaluate the NTTF electrode activity exemplified by MO degradation. As shown in Fig. 7, the degradation rate of MO increased as a function of bias potential. It was clearly observed that the applied bias potential of 2.0 V provided the most powerful way to degrade the MO in aqueous solution. The complete removal of MO was observed after 40 min, while only 78.3 and 36.3% of the MO degradation were obtained at the applied bias potential of 0.5 and 0 V, respectively. Furthermore, it was found that the experimental data approximately fit a pseudo-first-order kinetic model with the linear logarithmic expression: $\ln(C_o/C) = kt$; where $C_o$, $C$, and $k$ are the initial MO concentration, MO concentration at reaction time, $t$, and rate constant, individually. As shown in Table 2, the reaction rate for system receiving 2 V applied bias potential (e.g., $2.29 \times 10^{-3}$ $s^{-1}$) was about 10 times greater than that of 0 V condition (e.g., $1.52 \times 10^{-4}$ $s^{-1}$) at the same degree of illumination. Since the light intensity was equivalent in these two cases, the degree of photocatalysis should be equal. The difference may be due to the

**Table 2**
Pseudo-first-order rates of MO degradation ($k'_{obs}$) under different processes.

| | Rate constant ($k'_{obs}$, $s^{-1}$) | $R^2$ |
|---|---|---|
| Processes | | |
| PEC | $2.29 \times 10^{-3}$ | 0.9572 |
| EC | $1.52 \times 10^{-4}$ | 0.9275 |
| PC | $6.83 \times 10^{-5}$ | 0.9214 |
| P | $1.67 \times 10^{-5}$ | 0.9403 |
| Different bias potentials (V) | | |
| 0 | $1.52 \times 10^{-4}$ | 0.9275 |
| 0.5 | $5.00 \times 10^{-4}$ | 0.9495 |
| 1.0 | $7.37 \times 10^{-4}$ | 0.9677 |
| 1.5 | $1.53 \times 10^{-3}$ | 0.9026 |
| 2.0 | $2.29 \times 10^{-3}$ | 0.9572 |

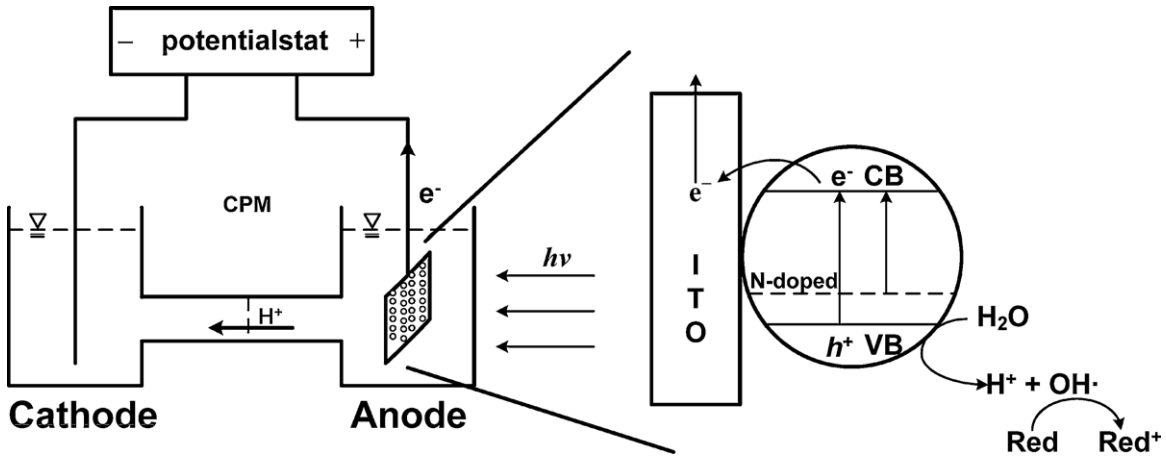


**Fig. 8.** Conceptual presentation of the degradation of MO by PEC method over NTTF.

following two main reasons. First, the greater the external (anodic) potential was applied, the greater the (anodic) current was generated. As a result, the system could undertake direct and indirect electrochemical oxidations of MO, e.g., $MO \rightarrow MO^+ + e^-$ and oxygen evolution, i.e., $H_2O \rightarrow O_2 + 4H^+ + 4e^-$. Second, greater external (anodic) potential could enhance the separation of photogenerated holes and electrons which enabled the accumulation of hole, a strong oxidant, on the photoanode surface for the oxidation of MO. The total electrons ($e_T^-$) in the PEC system can be described as:

$$e_T^- = e_{NTTF}^- + e_b^- \quad (4)$$

where $e_{NTTF}^-$ is the electrons generated from the NTTF after excited by light and $e_b^-$ is the electrons generated from the bias potential ($e_b^- = V_b/R$, where $V_b$ is bias potential, $R$ is system resistance). The system resistance ($R$) is fixed, so the $e_b^-$ is proportion to $V_b$. In other words, the $e_b^-$ can be obtained by testing different bias potentials vs. currents without illumination, i.e., the dark current at different bias potentials (shown in Table 1). As a result, the $e_{NTTF}^-$ can be calculated by the Eq. (4), and had values of 0.07, 0.20, 0.22, 0.34, 0.58 and 0.60 mA at the bias potential of 0.3, 0.5 0.7, 1.0, 1.5 and 2.0 V, correspondingly. In general, the photocurrent should be the same under the same degree of irradiation for the NTTF. However, the photocurrents, in this study, increased with the increase in bias potential. This suggested that the greater the increase in bias potential, which is a kind of driven force for electrons, the greater the decrease in recombination of electrons and holes. Meanwhile, applying larger external potential can provide greater anodic current to promote electrochemical oxidation reaction in the anode chamber. Our results were consistent with the findings of Zhao and Zhu [44] that PCE method could effectively degrade aqueous pollutants by the synergetic effect of electrochemical oxidation and photocatalytic oxidation. This study not only successfully proved the concept of synergetic effect in two-chamber PCE system, but also quantified the effect of photogenerated currents and holes on photoelectrochemical oxidation for the first time.

### 3.5. Mechanistic aspects

Hoffmann et al. [2] have described the elemental steps involved in the photoelectrochemical process in details. Briefly, the photogenerated hole is powerful oxidant (+1.0 to +3.5 V vs. NHE depending on the pH and type of semiconductor), while the photogenerated electron is strong reductant (+0.5 to −1.5 V vs. NHE) [56]. Most photodegradation reactions utilize the oxidation power of the hole either directly or indirectly; however, to prevent a buildup of degradation byproducts one must also provide a reducible species as electron scavengers. Herein, in this study, as depicted in above sections, a PEC system was applied to deal with this issue. Fig. 8 presents the schematic diagram of H-type electrochemical cell and the conceptual reaction pathway of the photoelectrochemical oxidation of MO over NTTF. In the anodic chamber, the MO molecules first diffuse to the NTTF surface and then become absorbed on the photoanode. When a photon with energy equal to or greater than the bandgap energy, $E_g$, of the photocatalyst, namely, NTTF, electrons are excited and jump from the valence band to the conduction band leaving behind a hole. In general, in the absence of hole or electron scavenger, the photogenerated electrons and holes recombine rapidly. As a result, the trapped holes will exhibit decreased oxidation efficiency. In a PEC system, in the presence of a bias potential, the photogenerated electrons will transfer to the cathode thereby reducing the hole–electron recombination. Notably, the current increases as the bias potential increases. But the current is contributed by photogenerated electrons rather than from the bias potential, which merely works as an electron pump that transports the electrons from the working to the counter electrode.

Electron spin resonance (ESR) studies have confirmed the existence of hydroxyl and hydroperoxy radicals in aqueous solutions of illuminated $TiO_2$ [2,57]. The valence-band hole will react with $H_2O$ to generate $OH^\bullet$ (i.e., surface-bound hydroxyl radical). Furthermore, the strong correlation between degradation rate and surface concentration of the organic pollutant [2,58,59] also suggests that the trapped holes or hydroxyl radicals are available at the surface of the photoanode [2]. It is commonly agreed that hydroxyl radical driving oxidation is the main mode for indirect electrochemical degradation of organic contaminants. [44,60,61]:

$$NTTF + H_2O \xrightarrow{h\nu} NTTF(^\bullet OH) + H^+ + e^- \quad (5)$$

$$NTTF(^\bullet OH) + R \rightarrow NTTF(OH) + R^\bullet \quad (6)$$

$$NTTF(^\bullet OH) + R^\bullet \rightarrow DPs + CO_2 + H^+ + e^- \quad (7)$$

$$NTTF(^\bullet OH) + R \rightarrow 0.5O_2 + e^- + NTTF \quad (8)$$

where, R represents methyl orange (MO) in this study and DPs refer to degradation products. Thus, the MO in the anodic chamber would be oxidized either directly or indirectly by this powerful oxidant, hydroxyl radical. In contrast to single chamber PEC system, reduction reaction rarely occurred in the anodic chamber because most electrons were transferred to the cathode (see as Fig. 8). This phenomenon suggests that two-chamber PEC system is favorable for the simultaneous utilization of photogenerated holes and electrons. Electrochemical oxidation also contributes to MO degradation through the oxygen generated to some extents (as Eq. (7)). Therefore, two-chamber PEC system enhances oxidation reaction

via the combination of electrochemical and photocatalytic reactions.

## 4. Conclusion

A nitrogen doped $TiO_2$ thin film (NTTF) was synthesized using the pulsed laser deposition method. The prepared NTFF was characterized using XRD, UV–vis absorbance edges, SEM, and XPS. After sintered at 600 °C, the NTTF was dominated by anatase phase, according to the XRD results matched with JCPDS-784486. An amount of 3 at% of N was doped into the NTTF structure by the linkage of Ti—O—N and N—Ti—O bond, leading to the absorbance shoulders exhibited at wavelength of 595 nm, which indicated that NTTF could be excited in visible light region. In addition, the nitrogen-doped $TiO_2$ nanoparticles spread uniformly over the ITO glass surface which is favorable for photoelectrochemical applications. Incident photon conversion efficiency (IPCE ($\lambda$)) was applied to evaluate the photoelectrochemical efficiency of NTTF. The highest photo-response was obtained at 325 nm, i.e., the maximum IPCE ($\lambda$) value of 26.77% was observed at the irradiation of 325 nm and a bias potential of 2.0 V. This material was then used as a photoanode in the photoelectrochemical system. Among photoelectrochemical, photocatalytic, electrochemical and photolysis methods, PEC showed the most efficient way in degrading methyl orange. The synergetic effect between electrochemical and photocatalytic method was quantified as 0.07 mA at 0.3 V bias potential and 0.6 mA at 2.0 V bias potential, respectively. In the present PEC system, most electrons were transferred to the cathode, which can minimize the recombination of photogenerated electrons and holes thereby increase the photoefficiency and enables the simultaneous utilization of photogenerated holes and electrons for performing separate oxidation and reduction reactions.

## Acknowledgments

The senior author wishes to thank National Science Council in Taiwan for the grant of Fellowship (NSC98291 7I564109). Professor J.H. Choi of Kongju National University in Korea provided excellent comments on the CV plots. Po-Yen Wang assisted us with PEC experiments.

## References

[1] A. Hagfeldt, M. Gratzel, Chemical Reviews 95 (1995) 49–68.
[2] M.R. Hoffmann, S.T. Martin, W.Y. Choi, D.W. Bahnemann, Chemical Reviews 95 (1995) 69–96.
[3] A.L. Linsebigler, G.Q. Lu, J.T. Yates, Chemical Reviews 95 (1995) 735–758.
[4] G. Rothenberger, J. Moser, M. Gratzel, N. Serpone, D.K. Sharma, Journal of the American Chemical Society 107 (1985) 8054–8059.
[5] J.C. Tristao, F. Magalhaes, P. Corio, M.T.C. Sansiviero, Journal of Photochemistry and Photobiology A: Chemistry 181 (2006) 152–157.
[6] A. Kongkanand, K. Tvrdy, K. Takechi, M. Kuno, P.V. Kamat, Journal of the American Chemical Society 130 (2008) 4007–4015.
[7] H. Lin, C.P. Huang, W. Li, C. Ni, S.I. Shah, Y.-H. Tseng, Applied Catalysis B: Environmental 68 (2006) 1–11.
[8] K.M. Parida, N. Sahu, A.K. Tripathi, V.S. Kamble, Environmental Science and Technology 44 (2010) 4155–4160.
[9] Y. Bai, Y. Cao, J. Zhang, M. Wang, R. Li, P. Wang, S.M. Zakeeruddin, M. Gratzel, Nature Materials 7 (2008) 626–630.
[10] X. Chen, S.S. Mao, Chemical Reviews 107 (2007) 2891–2959.
[11] R. Asahi, T. Morikawa, T. Ohwaki, K. Aoki, Y. Taga, Science 293 (2001) 269–271.
[12] B. Farkas, J. Budai, I. Kabalci, P. Heszler, Z. Geretovszky, Applied Surface Science 254 (2008) 3484–3488.
[13] T. Lindgren, J.M. Mwabora, E. Avendano, J. Jonsson, A. Hoel, C.G. Granqvist, S.E. Lindquist, Journal of Physical Chemistry B 107 (2003) 5709–5716.
[14] S.H. Lee, E. Yamasue, K.N. Ishihara, H. Okumura, Applied Catalysis B: Environmental 93 (2010) 217–226.
[15] Y.P. Peng, S.L. Lo, F.H. Ou, S.W. Lai, Journal of Hazardous Materials 183 (2010) 754–758.
[16] Y. Suda, H. Kawasaki, T. Ueda, T. Ohshima, Thin Solid Films 453–454 (2004) 162–166.
[17] Y. Suda, H. Kawasaki, T. Ueda, T. Ohshima, Thin Solid Films 475 (2005) 337–341.
[18] L. Zhao, Q. Jiang, J. Lian, Applied Surface Science 254 (2008) 4620–4625.
[19] N. Sato, M. Matsuda, M. Yoshinaga, T. Nakamura, S. Sato, A. Muramatsu, Topics in Catalysis 52 (2009) 1592–1597.
[20] G. Socol, Y. Gnatyuk, N. Stefan, N. Smirnova, V. Djokic, C. Sutan, V. Malinovschi, A. Stanculescu, O. Korduban, I.N. Mihailescu, Thin Solid Films 518 (2010) 4648–4653.
[21] N. Ozer, H. Demiryont, J.H. Simmons, Applied Optics 30 (1991) 3661–3666.
[22] J.A. Byrne, B.R. Eggins, S. Linquette-Mailley, P.S.M. Dunlop, Analyst 123 (1998) 2007–2012.
[23] N. Rausch, E.P. Burte, Journal of the Electrochemical Society 140 (1993) 145–149.
[24] T. Nakamura, T. Ichitsubo, E. Matsubara, A. Muramatsu, N. Sato, H. Takahashi, Acta Materialia 53 (2005) 323–329.
[25] H. Lin, A.K. Rumaiz, M. Schulz, D. Wang, R. Rock, C.P. Huang, S.I. Shah, Materials Science and Engineering: B 151 (2008) 133–139.
[26] E. Gyorgy, G. Socol, E. Axente, I.N. Mihailescu, C. Ducu, S. Ciuca, Applied Surface Science 247 (2005) 429–433.
[27] V.C. Nogueira, C. Longo, A.F. Nogueira, M.A. Soto-Oviedo, M.A. De Paoli, Journal of Photochemistry and Photobiology A: Chemistry 181 (2006) 226–232.
[28] S. Nakade, T. Kanzaki, S. Kambe, Y.J. Wada, S. Yanagida, Langmuir 21 (2005) 11414–11417.
[29] B. Zhou, M. Schulz, H.Y. Lin, S.I. Shah, J.H. Qu, C.P. Huang, Applied Catalysis B: Environmental 92 (2009) 41–49.
[30] O. Khaselev, J.A. Turner, Science 280 (1998) 425–427.
[31] Y. Sun, C.J. Murphy, K.R. Reyes-Gil, E.A. Reyes-Garcia, J.P. Lilly, D. Raftery, International Journal of Hydrogen Energy 33 (2008) 5967–5974.
[32] A. Wolcott, W.A. Smith, T.R. Kuykendall, Y.P. Zhao, J.Z. Zhang, Advanced Functional Materials 19 (2009) 1849–1856.
[33] M. Halmann, Nature 275 (1978) 115–116.
[34] T. Inoue, A. Fujishima, S. Konishi, K. Honda, Nature 277 (1979) 637–638.
[35] E.B. Cole, P.S. Lakkaraju, D.M. Rampulla, A.J. Morris, E. Abelev, A.B. Bocarsly, Journal of the American Chemical Society 132 (2010) 11539–11551.
[36] T. Arai, S. Sato, K. Uemura, T. Morikawa, T. Kajino, T. Motohiro, Chemical Communications 46 (2010) 6944–6946.
[37] V. Subramanian, E. Wolf, P.V. Kamat, Journal of Physical Chemistry B 105 (2001) 11439–11446.
[38] D.C. Schmelling, K.A. Gray, P.V. Kamat, Environmental Science and Technology 30 (1996) 2547–2555.
[39] D.L. Jiang, S.Q. Zhang, H.J. Zhao, Environmental Science and Technology 41 (2007) 303–308.
[40] S. Somasundaram, C.R. Chenthamarakshan, N.R. de Tacconi, Y. Ming, K. Rajeshwar, Chemistry of Materials 16 (2004) 3846–3852.
[41] S.H. Xiao, J.H. Qu, X. Zhao, H.J. Liu, D.J. Wan, Water Research 43 (2009) 1432–1440.
[42] X.F. Cheng, W.H. Leng, D.P. Liu, Y.M. Xu, J.Q. Zhang, C.N. Cao, Journal of Physical Chemistry C 112 (2008) 8725–8734.
[43] Z.H. Zhang, Y. Yuan, G.Y. Shi, Y.J. Fang, L.H. Liang, H.C. Ding, L.T. Jin, Environmental Science and Technology 41 (2007) 6259–6263.
[44] X. Zhao, Y.F. Zhu, Environmental Science and Technology 40 (2006) 3367–3372.
[45] R.T. Pelegrini, R.S. Freire, N. Duran, R. Bertazzoli, Environmental Science and Technology 35 (2001) 2849–2853.
[46] X. Zhao, J.H. Qu, H.J. Liu, C. Hu, Environmental Science and Technology 41 (2007) 6802–6807.
[47] M. Gopal, W.J.M. Chan, L.C. DeJonghe, Journal of Materials Science 32 (1997) 6001–6008.
[48] J.I. Pankove, Optical Process in Semiconductors, Dover Publications, NJ, 1971.
[49] G.S. Shao, F.Y. Wang, T.Z. Ren, Y.P. Liu, Z.Y. Yuan, Applied Catalysis B: Environmental 92 (2009) 61–67.
[50] M. Bellardita, M. Addamo, A. Di Paola, L. Palmisano, A.M. Venezia, Physical Chemistry Chemical Physics 11 (2009) 4084–4093.
[51] H.-H. Ou, S.-L. Lo, C.-H. Liao, The Journal of Physical Chemistry C 115 (2011) 4000–4007.
[52] S. Livraghi, M.R. Chierotti, E. Giamello, G. Magnacca, M.C. Paganini, G. Cappelletti, C.L. Bianchi, The Journal of Physical Chemistry C 112 (2008) 17244–17252.
[53] H. Irie, Y. Watanabe, K. Hashimoto, Journal of Physical Chemistry B 107 (2003) 5483–5486.
[54] Y.P. Peng, Y.T. Yeh, S.I. Shah, C.P. Huang, Applied Catalysis B: Environmental 123-124 (2012) 414–423.
[55] Y.I. Hou, J.H. Qu, X. Zhao, P.J. Lei, D.J. Wan, C.P. Huang, Science of the Total Environment 407 (2009) 2431–2439.
[56] M. Gratzel, Heterogeneous Photochemical Electron Transfer, CRC Press, Boca Raton, FL, 1989.
[57] C.D. Jaeger, A.J. Bard, The Journal of Physical Chemistry 83 (1979) 3146–3152.
[58] S. Tunesi, M. Anderson, The Journal of Physical Chemistry 95 (1991) 3399–3405.
[59] C. Kormann, D.W. Bahnemann, M.R. Hoffmann, Environmental Science and Technology 25 (1991) 494–500.
[60] M. Zhou, Q. Dai, L. Lei, C.a. Ma, D. Wang, Environmental Science and Technology 39 (2004) 363–370.
[61] J.M. Kesselman, N.S. Lewis, M.R. Hoffmann, Environmental Science and Technology 31 (1997) 2298–2302.